Teknomekanik, Vol. 9, No. 1, pp. 1-24, February 2026
e-ISSN: 2621-8720 p-ISSN: 2621-9980

Comparative analysis of bio-inspired and topology-optimized lattices under compressive loading

Ahmad Anas Arifin[1], I Made Londen Batan[1*], Michele Bici[2], Arif Wahjudi[1] and Agus Sigit Pramono[1]

[1] Department of Mechanical Engineering, Institut Teknologi Sepuluh Nopember, **Indonesia**
[2] Department of Mechanical and Aerospace Engineering, Sapienza University of Rome, **Italy**

* Corresponding Author: londbatan@me.its.ac.id
Received: 09 September 2025; *Revised:* 25 November 2025; *Accepted:* 20 December 2025

Cite this https://doi.org/10.24036/teknomekanik.v9i1.45472

Abstract: Lattice structure design is still dominated by strut-based forms and surface-based shapes, such as triply periodic minimal surfaces (TPMS), which both exhibit overlapping limitations. Strut lattices often show strong anisotropy because their response depends heavily on cell orientation, while TPMS lattices are difficult to adjust when bounded by geometric constraints. These conditions eventually led to stagnation in the development of lattice morphology. Hybrid and topology-optimization methods have appeared as possible alternatives, but many of them still produce modified versions of classical patterns. This study examined two lattice geometries: the Pyramorph, inspired by the shape of a pyramid, and the Topomorph, generated through a topology optimization framework. Both structures were designed using a CAD unit cell patterning technique and manufactured using the FDM method, with relative densities ranging from 0.40 to 0.44. Their mechanical behaviour was examined through FEA simulation and uniaxial compression testing. The parameter variations included cell orientations of 0°, 15°, 30°, and 45°, and cell sizes of 8 mm and 12 mm within a 24 mm specimen. The Topomorph showed superior strength, reaching 15–20 MPa, while the Pyramorph reached only 7–8 MPa. The highest value, about 20.5 MPa, was obtained from the Topomorph at 0° and with an 8 mm cell size. Failure modes indicated buckling and delamination in the Pyramorph, while the Topomorph tended to collapse progressively. These findings indicate that topology optimization combined with CAD-based patterning could significantly improve lattice performance.

Keywords: lattice structures; topology optimization; compressive behaviour; material engineering

1. Introduction

The development of advanced lattice structures has become a focal point in materials engineering, offering exceptional strength-to-weight ratios for aerospace, biomedical, and automotive applications [1][2]. Lattice structures can be classified into several categories based on the unit cell and the replication pattern [3]. Based on the unit cell, lattices can be either surface-based or strut-based. Meanwhile, in terms of replication patterns, lattices can be replicated as regular, pseudo-regular, and stochastic [4]. Each category serves specific functional requirements depending on the strategy and conditions that will be applied to the lattice structure.

Strut-based lattice cells are generally formed from basic cylindrical struts arranged within a cubic domain. For instance, a Body-centered Cubic (BCC) lattice is formed from eight struts extending diagonally from the top plane to the bottom plane [5]. The mechanical performance of the lattice is strongly influenced by its relative density, which is primarily controlled by the strut cross-sectional diameter. The larger the diameter, the greater the relative density, and the higher the stiffness of the lattice cell. Meanwhile, in the surface-based lattice cells, the relative density is adjusted using

the thickness of the surface. The thicker it is, the higher the relative density, as well as the stiffness and strength [6].

However, relative density does not fully determine the overall mechanical properties of a lattice cell. Another key influencing factor is unit cell geometry. For example, previous research on lattice cells of Simple Cubic (SC), BCC, Face-centered Cubic (FCC) types with the same relative density demonstrated significant differences in stiffness and strength [7]. These effects can be illustrated in the 3D spatial Young's modulus of each lattice cell shape [7], [8], [9]. These findings indicate that the shape of the cell can affect its strength of the cell. This finding suggests opportunities for exploring novel cell geometries with tailored mechanical properties.

Biomimicry and topology optimization are usually used to discover new shapes that differ from existing forms, including strut- and surface-based lattices. Biomimicry can reveal shapes inspired by natural and historical structures, such as animals, plants, or ancient structures. For example, the shape of sea urchins is used to create a cell lattice design with isotropic properties (having the same mechanical properties in all directions) [10]. This technique is practical but requires additional post-processing steps before implementation. The second method is to use topology optimization to generate a shape according to the predetermined boundary conditions. Usually, topology optimization typically employs objective functions targeting volume fraction or mass reduction [11][12]. One of the commonly used techniques is SIMP (Solid Isotropy Microstructure with Penalization) [13]. The advantage of this technique is that it can provide boundary conditions according to the usage requirements. However, this technique requires a considerable amount of resources and time because the generated shape cannot be used directly; requires extensive refinement before use [11].

Both techniques require additional processes to be used in creating new lattice shapes. These processes are related to Computer-aided Design (CAD) re-interpretation and patterning. This process allows biomimetic shapes to be directly used as cell lattices, and the topology optimization process becomes faster because the boundary condition is only applied to one plane. This requirement for lattice structures is cubic symmetry, which means that the unit cell has identical shape symmetry along the three axes: X, Y, and Z. This symmetry ensures consistent mechanical properties of the lattice unit cell the same along the three axes X, Y, and Z. To address the research gap between the application of biomimetic techniques and topology optimization in generating unit cell lattices, a CAD interpretation and patterning technique is introduced in this paper as a CAD Unit Cell Patterning technique.

This paper applies the CAD Unit Cell Patterning technique to two types of lattice unit cells: the Pyramorph, which emulates the fundamental shape of the Egyptian pyramid, and the Topomorph, which is generated through topology optimization under a single load plane. The constructed unit cell lattice will be designed with the same relative density for later compression testing. This study evaluates the mechanical properties of the unit cell lattice by testing it in various orientations and cell sizes. The evaluation will be performed experimentally and by numerical simulation employing the finite element analysis technique.

Although biomimetic lattice structures and topology optimization have been extensively researched, comparative studies remain limited, comparing these two types of lattices under controlled relative densities and varying load orientations. Additionally, the shapes of the resulting TO products tend to require more post-processing steps and are often not cubically symmetric, thus limiting their use as unit cells. Therefore, to fill this gap, this research is designed with identical relative densities as the CAD Unit Cell Patterning method, which can generate symmetric and readily manufacturable unit cell lattice shapes for lattice forms resulting from biomimetic processes or topology optimization. The principal contributions of this study include:

(i) Developing two new lattice geometries (Pyramorph and Topomorph)
(ii) Establishing a CAD patterning technique applicable to biomimicry-derived and topology-optimized lattices, and
(iii) Providing the first experimental comparison of these geometries in controlling cell orientation and size with uniform specimen relative density.

This work presents a more straightforward and manufacturable approach using the CAD Unit Cell Patterning method, in contrast to earlier works on topology-optimized or biomimetic lattices, which usually required extensive post-processing, multi-stage smoothing, or complex boundary-condition optimization. This technique enables both biomimetic and topology-optimized shapes to be converted into cubic-symmetric unit cells without the need for additional geometry healing or re-meshing. Furthermore, unlike earlier studies that evaluated only a single topology or relied solely on numerical predictions, the present work provides a controlled experimental comparison between two distinctly generated lattice morphologies, Pyramorph and Topomorph using identical relative densities, orientations, and cell sizes.

2. Material and methods

2.1 Design of unit cell

This study focuses on the design and development of two lattice structures: the Pyramorph Lattice, inspired by the geometry of Egyptian pyramids, and the Topomorph Lattice, generated through topology optimization. Both models were designed with careful consideration of symmetry, structural efficiency, and mathematical precision. The Pyramorph Lattice was developed as the initial model, drawing inspiration from the stability and symmetry of pyramid shapes. The design process began with a cubic domain of dimensions $2a\ x\ 2a\ x\ 2a$. Two pyramids joined at their bases and bisected at the midplane formed a truncated octahedron in the middle of the cube. This central structure was mathematically defined by Equation (1) [14][15].

$$\frac{|x|}{a}+\frac{|y|}{a}+\frac{|z|}{a}\leq 1 \tag{1}$$

From this core, six central pyramids were created, each pointing along the X+, X-, Y+, Y-, Z+, and Z- directions. Each pyramid was defined by Equation (2).

$$\frac{|x-x_i|}{a}+\frac{|y-y_i|}{a}+\frac{|z-z_i|}{a}=1 \tag{2}$$

where (x_i, y_i, z_i) represents the coordinates of the pyramid's apex. To enhance structural integrity, eight additional pyramids were added at the cube's corners [16]. These corner pyramids were defined by equation (3).

$$\frac{|x-x_j|}{a}+\frac{|y-y_j|}{a}+\frac{|z-z_j|}{a}=1 \tag{3}$$

where (x_j, y_j, z_j) are the coordinates of the cube's corners. This configuration ensured geometric symmetry and load balance across all three principal planes (XY, XZ, YZ). The detailed unit-cell geometry is shown in Figure 1. The relative density (Φ) of this unit cell was calculated by equation (4)[16][17]. The value of relative density for pyramorph is 0.4.

$$\Phi=\frac{V_L}{V_s} \tag{4}$$

The second model, the Topomorph Lattice, was developed using topology optimization to enhance structural efficiency. A cube of the same dimensions $2a\ x\ 2a\ x\ 2a$ was used as the design domain.

Three loading conditions were applied: a normal force on the top surface, a shear force on one side, and a torsional force to simulate twisting. The optimization process was performed using Altair Optistruct, with the objective of minimizing weight compliance while maximizing stiffness with 30% volume fraction constraint [18]. The resulting geometry was exported as an STL file and refined in CAD software for further development. The optimization result as shown in Figure 2. The CAD Unit Cell Patterning process for the Topomorph Lattice followed a similar approach to the Pyramorph Lattice. The optimized geometry from force and torque combination was divided into smaller, repeatable unit cells, ensuring symmetry across the X, Y, and Z axes. These unit cells were then replicated to form the complete lattice structure. To mathematically describe the lattice, MATLAB was used to analyze the surface and edge profiles. Curve-fitting techniques were applied to derive the governing equations, which included parameters such as node positions, edge equations, and surface equations.

In this study, MATLAB was exclusively used for geometric curve fitting, surface extraction, and the parametric analysis of unit-cell edges and profiles. Its work was limited to only rearranging the lattice geometry, without being used to estimate material response or predict its mechanical strength. The use of mathematical curves and surface reconstruction as one of the design steps in lattice creation has been widely adopted in previous studies in the field of geometric modeling. It has been demonstrated that geometric extraction, functional surface representation, and curve/surface reconstruction constitute standard practices in lattice design workflows [19]. Therefore, the MATLAB process used in this study followed the established and verified method for creating lattice designs through computation. The purpose was to serve as a tool for geometric reconstruction, rather than a platform for simulation.

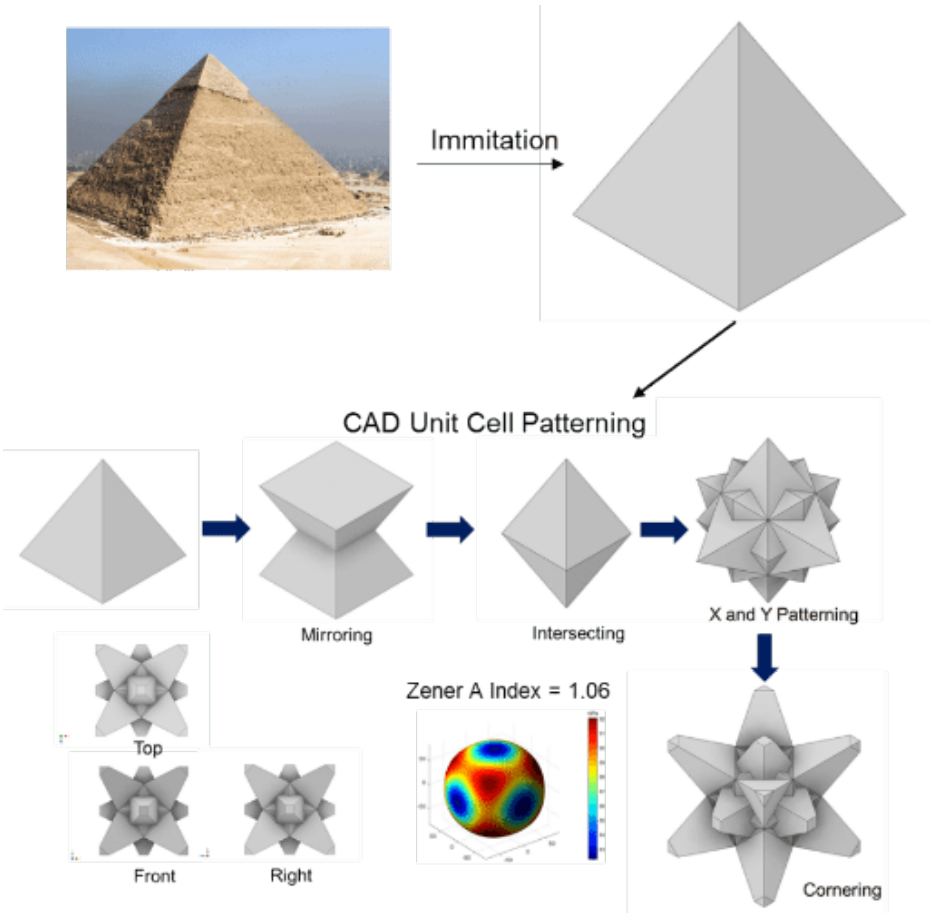

Figure 1. CAD unit cell patterning of Pyramorph Lattice

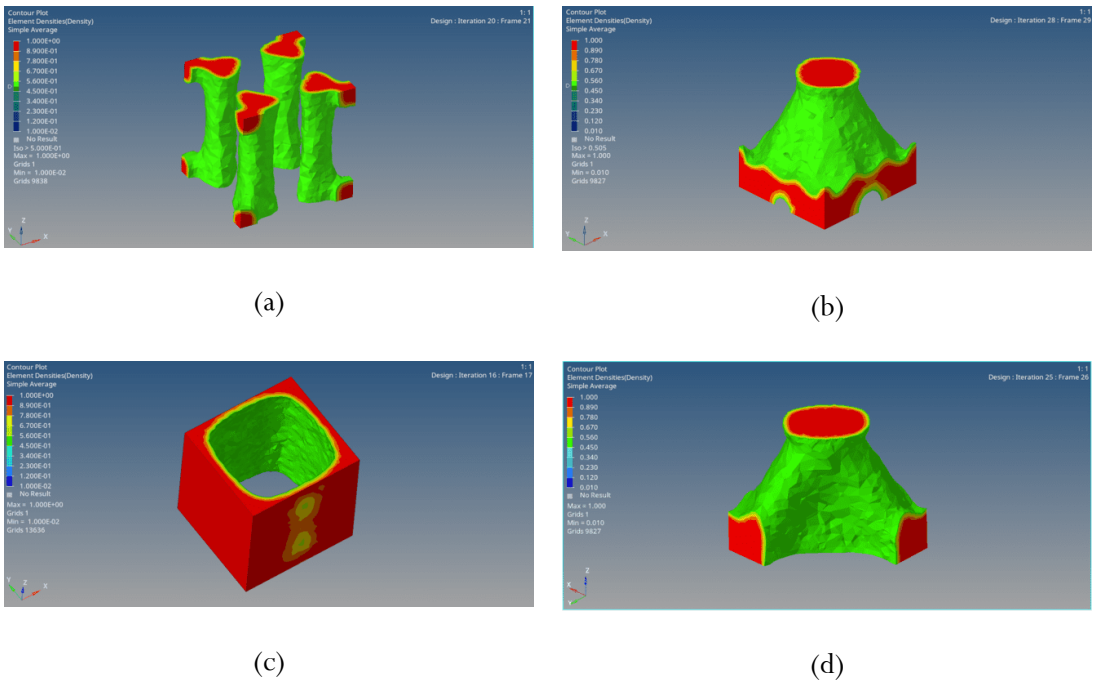

(a) (b)

(c) (d)

Figure 2. Topology optimization result of single load plane for input. (a) Force Z axis, (b) Force X or Y axis, (c) Torque/moment Z axis, and (d) Combination of force and torque

The Topomorph Lattice featured unique geometric elements, including circular patterns and shifted centers. Circles were defined on the XY, XZ, and YZ planes using the equations (5-7).

$$x = r\,cos(\theta), y = r\,sin(\theta), z = a\ (XY\ Plane) \tag{5}$$

$$x = r\,cos(\theta), z = r\,sin(\theta), y = a\ (XZ\ Plane) \tag{6}$$

$$y = r\,cos(\theta), z = r\,sin(\theta), z = a\ (YZ\ Plane) \tag{7}$$

where r is the radius and θ is the angle parameterization. Additionally, circles with shifted centers were introduced, defined by equation (8).

$$x = C + r_2\cos(\theta)\,, z = C + r_2\cos(\theta)\,, y = 0 \tag{8}$$

where $r_2 = 0.3125a$ and center shift $C = \frac{2.828a}{5}$. Detail mathematical model is presented in Figure 3. Meanwhile, the complete CAD unit-cell patterning process is shown in Figure 4.

Equations 5 to 8 represent the mathematical interpretation of the geometric form of the unit cell lattice type Topomorph developed in this study. These equations were derived directly from mapping the CAD model by identifying its circular and shifted-center patterns in their parametric form. The equations were newly derived in this study where their creation process followed the standard formulation of the parametric circle equation commonly used in computational geometry. The use of mathematical representations in the process of converting CAD geometry into analysis functions is a common practice in geometric modeling workflows, as described in Piegl and Tiller's NURBS framework [20]. In this study, these equations were used only to reconstruct and visualize the lattice geometry without being used to predict its mechanical behaviour.

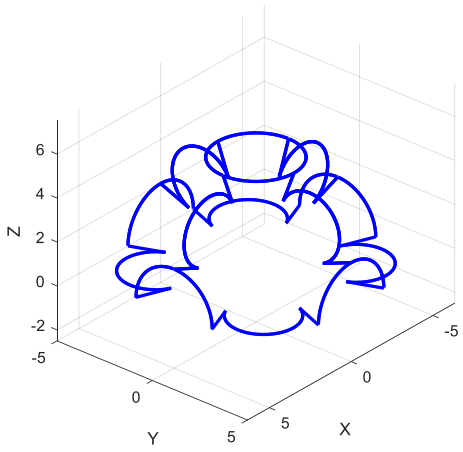

Figure 3. Mathematical model of Topomorph Lattice

The Topomorph Lattice was further optimized by introducing through-holes on the XY, XZ, and YZ planes. These holes were designed to reduce the relative density of the lattice while maintaining its mechanical properties, particularly in the normal direction. The diameter of the holes was determined by the ratio $\frac{r}{2a}$, where r is the radius of the hole and $2a$ is the edge length of the cubic unit cell. In this study, the hole ratio was set to $\frac{3}{2a}$, which was chosen to achieve an optimal balance between mass reduction and structural integrity. The relative density of unit topomorph cell for $hole = \frac{3}{2a}$ was 0.4, the same value as the Pyramorph lattice. This set value was important to enable a comparative study between two lattices.

The introduction of through-holes significantly reduced the relative density of the lattice without compromising its mechanical performance. This was validated by calculating the Zener anisotropy index, a dimensionless parameter that quantifies the degree of anisotropy in a material's elastic properties. A Zener index of 0.6 was achieved, indicating that the lattice maintains a relatively low level of anisotropy. This is particularly advantageous for the intended compression test, as it ensures that the lattice exhibits superior mechanical properties in the normal direction compared to the shear direction. Detail scheme of optimization based on hole ratio as shown in Figure 5.

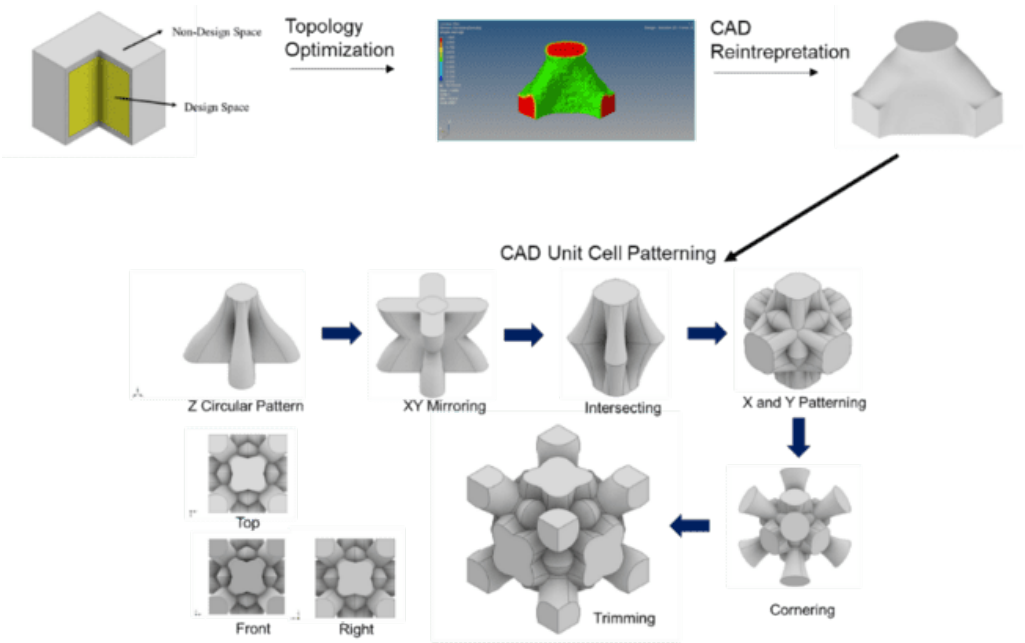

Figure 4. CAD unit cell patterning of Topomorph Lattice

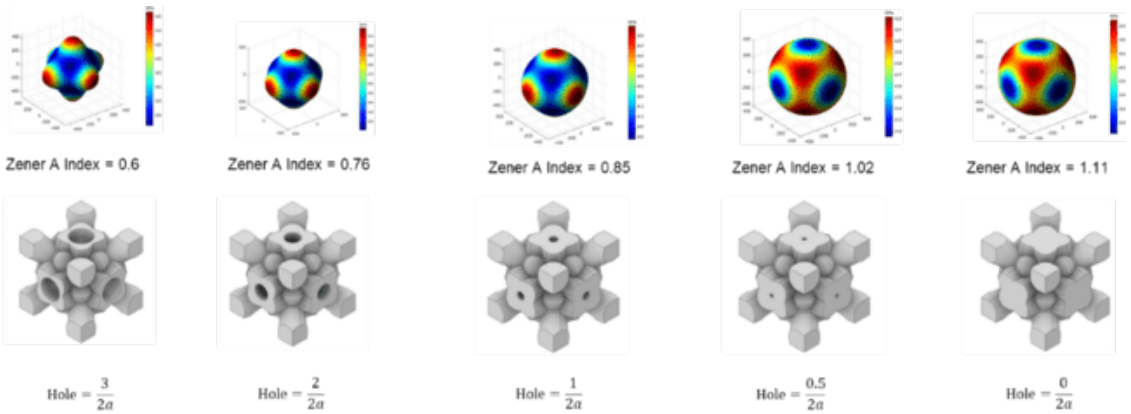

Figure 5. Hole-based optimization of Topomorph Lattice

In general, the CAD Unit Cell Patterning Technique flowchart as shown in Figure 6. This technique can be applied to all CAD-based forms that are then transformed into a unit cell lattice ready for replication and tessellation. The technique focuses on lattices that are isometric in all three planes.

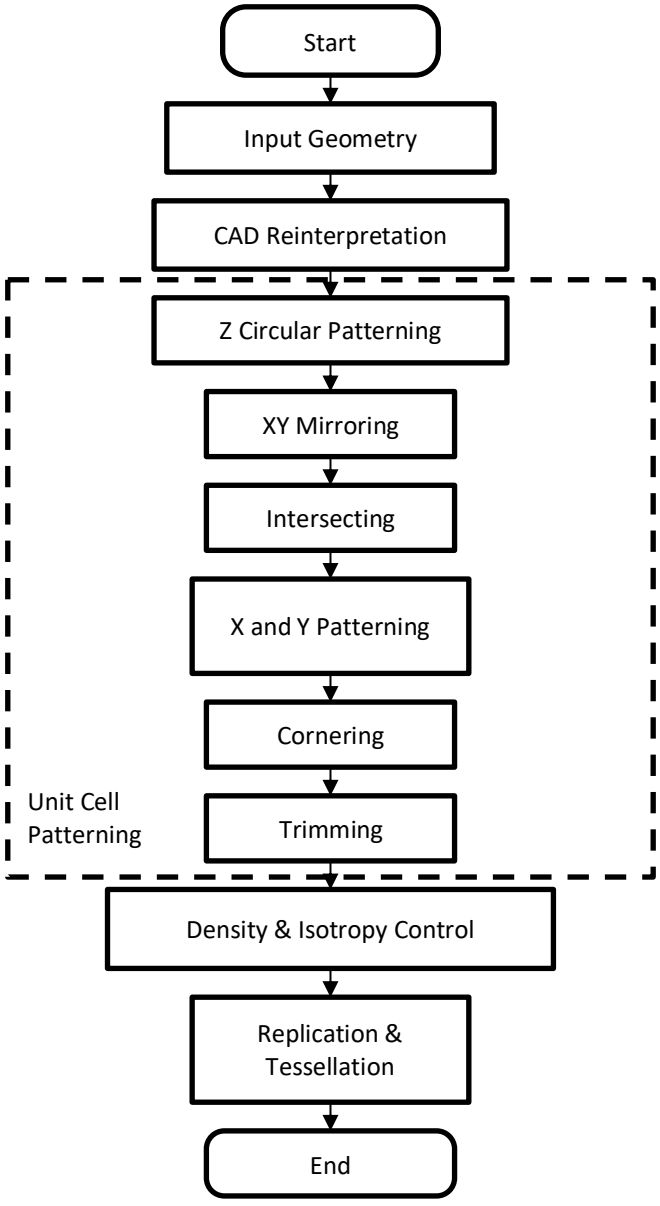

Figure 6. Flowchart of CAD unit cell patterning technique

2.2 Additive manufacturing processes

In this study, additive manufacturing (AM) technology was employed to fabricate the lattice structures. Specifically, the Fused Deposition Modeling (FDM) technique was utilized, which is one of the most widely used AM methods due to its cost-effectiveness and versatility in producing complex geometries. The FDM machine used in this research was the Flashforge Creator Pro 2, manufactured by Zhejiang Flashforge 3D Technology Co., LTD. This machine operates with a 1.75 mm PLA (Polylactic Acid) filament from the eSun brand, a biodegradable thermoplastic known for its ease of use and environmental friendliness. The slicing process was conducted using Flashprint 5 ©, the proprietary software developed by Flashforge. This software enables precise control over the printing parameters, ensuring high-quality fabrication of the lattice structures. The following parameters were optimized for the printing process as shown as Table 1.

Table 1. Process parameters set for PLA filament

Parameter	Value
Print nozzle diameter (mm)	0.4
Nozzle Temperature (°C)	200-210
Bed Temperature (°C)	40
Layer height (mm)	0.18
Print infill (%)	100
Print Speed (mm/min)	60

These parameters were selected based on prior studies that highlight their effectiveness in achieving optimal mechanical properties and dimensional accuracy in FDM-printed parts. The PLA material used in this study has the following mechanical properties (Table 2). These properties make PLA a suitable material for prototyping and functional testing of lattice structures, as it provides a balance between strength, stiffness, and ease of processing. In previous studies on polymer lattice structures, such as those conducted by Kumar et al, PLA was also used as the main material [10]. PLA has proven to have reliable printability and predictable stress-strain response. This makes PLA a suitable material for evaluating and comparing lattice structures.

Table 2. Material properties of PLA filament

Properties	Value
Density (g/cm^3)	1.2
Young Modulus (MPa)	3500
Tensile stress yield (MPa)	63.2
Ultimate Tensile Strength (MPa)	65
Poisson's Ratio	0.36

These parameters were selected based on prior studies that highlight their effectiveness in achieving optimal mechanical properties and dimensional accuracy in FDM-printed parts. The PLA material used in this study has the following mechanical properties (Table 2). These properties make PLA a suitable material for prototyping and functional testing of lattice structures, as it provides a balance between strength, stiffness, and ease of processing.

2.3 Specimen design

The specimens for this study were designed to investigate the influence of cell size and cell orientation on the compressive strength of lattice structures. Two types of lattice structures were examined: the Pyramorph Lattice and the Topomorph Lattice. A total of 16 specimens were

prepared, with 8 specimens for each lattice type, each measuring 24 x 24 x 24 mm. Two cell sizes were selected: 8 mm and 12 mm, to analyze the effect of scaling on mechanical performance. The cell sizes of 8 mm and 12 mm were chosen due to constraints in the fabrication process and because they are common cell sizes used in the preparation of compression test specimens [10]. The size of the cells also makes the printing process using a 0.4 mm nozzle better, allowing for geometric resolution to be achieved and avoiding excessive slenderness. Smaller cells are expected to provide higher density and strength, while larger cells may reduce weight but compromise mechanical properties. Additionally, four orientation angles were tested: 0°, 15°, 30°, and 45°, to determine whether cell orientation influences load distribution and overall strength. This combination of cell sizes and orientations allows for a comprehensive analysis of their impact on compressive strength and the identification of optimal design parameters. Specimens can be found in Figures 7 and 8.

The design of the specimens was carefully planned to ensure consistency and reproducibility. Each lattice type was tested under the same conditions, with variations only in cell size and orientation. The goal was to systematically evaluate how these parameters affect the mechanical behaviour of the lattice structures, particularly their compressive strength. By varying cell size and orientation, this study aims to provide insights into the optimal design of lattice structures for applications requiring lightweight yet strong materials.

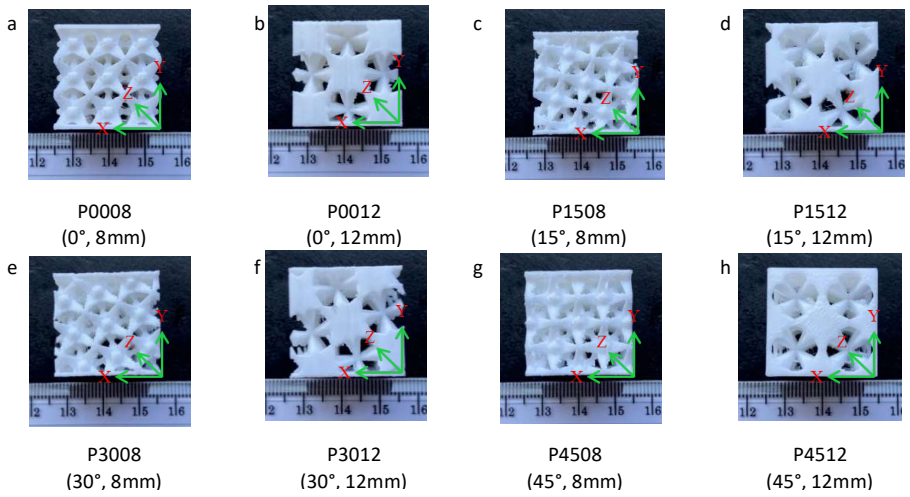

Figure 7. Pyramorph Lattice specimen

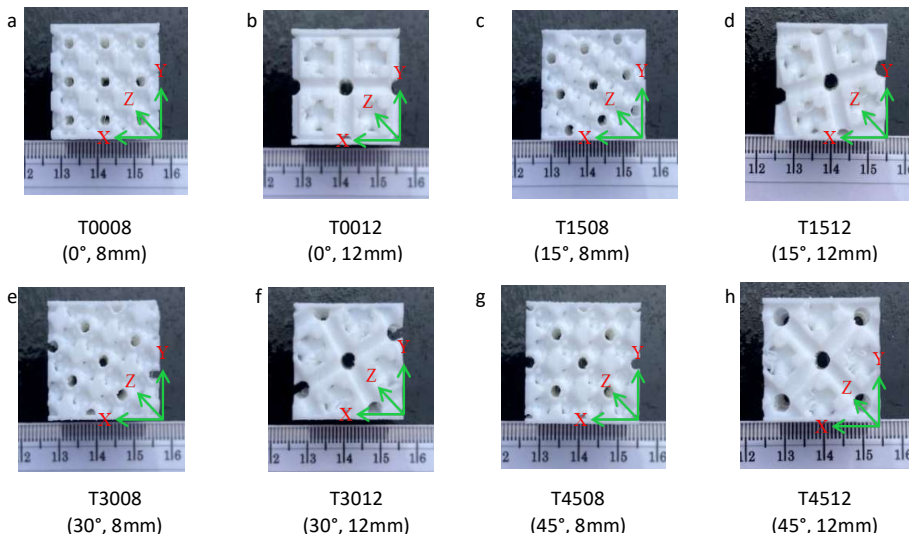

Figure 8. Topomorph Lattice specimen

2.4 Compression testing

The mechanical performance of the lattice structures was evaluated through uniaxial compression testing using a Universal Testing Machine (UTM) WDW-20E from Time Group Inc., equipped with a 20 kN load cell. The tests were conducted at a constant speed of 0.5 mm/min until the specimens reached a final deformation of 40% of their original height (h_0), with the compressive force applied perpendicular to the printing direction to assess anisotropic behaviour. The resulting load vs. displacement data was processed into stress-strain curves, where stress (σ) was calculated as the applied load divided by the cross-sectional area, and strain (ε) as the displacement divided by the original height. Additionally, the energy absorption capacity was determined using the integral of the stress-strain curve up to 40% deformation, providing insights into the lattice's ability to dissipate energy. Post-test visual inspection was performed to analyze failure mechanisms, such as buckling, strut fracture, or layer delamination, offering a comprehensive understanding of the deformation and failure behaviour of the lattice structures under compressive loading. Detail formula as shown as equation (9)-(12).

The compression tests conducted in this study were generally adapted from the ASTM D695 and ISO 604 standards commonly used for rigid polymeric materials. Despite this, there is still no international standard that can be specifically used for lattice or cellular structures. Some studies related to lattices have modified the testing standards of ASTM D695 to make them suitable for open-cell lattices and specimen dimensions [21], [22]. Similar adaptations were also applied to PLA-based lattice structures manufactured using FDM [23].

$$\sigma_{N,c} = \frac{P_c}{A_{0,eq}} \tag{9}$$

$$A_{0,eq} = \frac{V_L}{h_0} = (1-\phi){h_0}^2 \tag{10}$$

$$\varepsilon_{N,c} = \frac{u_c}{h_0} \tag{11}$$

$$W_c = \int_{\varepsilon=0}^{\varepsilon=0.4} \sigma_{N,c}\varepsilon_{N,c}\, d\varepsilon \tag{12}$$

The value of ε=0.4 is chosen because the graph that appears after that, starts to become unstable. The calculated values of $A_{0,eq}$ and ϕ as shown as Table 3 and 4.

Table 3. Equivalent cross section area of cell dan density on Pyramorph Lattice

Number of Specimen	Orientation (Deg)	Cell Size (mm)	Size h0 (mm)	Volume Lattice V_L (mm^3)	Volume Solid Cube V_s (mm^3)	Density Φ (%)	Equivalent Cross Section Area of Cell (mm^2)
P0008	0	8:8:8	24	6045.38	13824.00	0.43	251.89
P0012	0	12:12:12	24	5615.05	13824.00	0.40	233.96
P1508	15	8:8:8	24	5849.34	13824.00	0.42	243.72
P1512	15	12:12:12	24	5495.44	13824.00	0.39	228.98
P3008	30	8:8:8	24	5651.30	13824.00	0.40	235.47
P3012	30	12:12:12	24	5861.35	13824.00	0.42	244.22
P4508	45	8:8:8	24	5817.71	13824.00	0.42	242.40
P4512	45	12:12:12	24	6183.79	13824.00	0.44	257.66

Table 4. Equivalent cross section area of cell dan density on Topomorph Lattice

Number of Specimen	Orientation (Deg)	Cell Size (mm)	Size h0 (mm)	Volume Lattice V_L (mm^3)	Volume Solid Cube V_s (mm^3)	Density Φ (%)	Equivalent Cross Section Area of Cell (mm^2)
T0008	0	8:8:8	24	6050.38	13824.00	0.43	252.10
T0012	0	12:12:12	24	6198.54	13824.00	0.44	258.27
T1508	15	8:8:8	24	5835.54	13824.00	0.42	243.14
T1512	15	12:12:12	24	5854.23	13824.00	0.42	243.92
T3008	30	8:8:8	24	5845.67	13824.00	0.42	243.56
T3012	30	12:12:12	24	5897.43	13824.00	0.42	245.72
T4508	45	8:8:8	24	5832.54	13824.00	0.42	243.02
T4512	45	12:12:12	24	5851.35	13824.00	0.42	243.80

2.5 Finite element analysis

Finite element analysis (FEA) was employed for the numerical simulations conducted in this study. Tetrahedral elements with a uniform size of 0.4 mm were adopted for the meshing process, and an example of the generated mesh is presented in Figure 9. The bottom plane of the specimen was fully constrained, while a compressive force was applied to the top plane. No constraints were imposed on the lateral faces. In addition, the stress convergence criterion for the von Mises stress was maintained below 10% to ensure the accuracy of the simulation results. When the convergence threshold exceeded 10%, the mesh size was refined and the simulation was repeated. The material behavior was defined using linear elastic properties. The maximum load supported by the specimen was subsequently determined using Equations (13) and (14) in combination with the von Mises stress data obtained from the simulations.

$$F_{max} = \frac{\sigma_y \, x \, F_{input}}{\sigma_{actual}} \tag{13}$$

$$\sigma_{Compressive\ Strength} = \frac{F_{max}}{A} \tag{14}$$

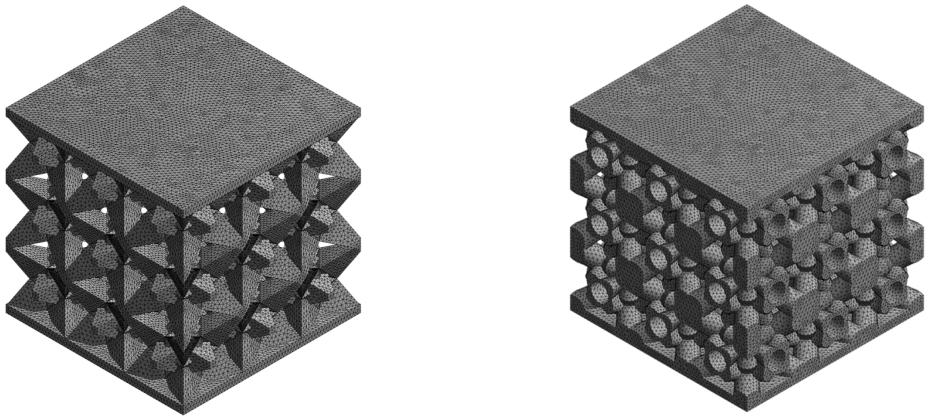

(a) (b)

Figure 9. Example of generated mesh of (a) Pyramorph and (b) Topomorph

3. Results and discussion

3.1 Failure mode

Lattice constructions typically break down under stress by bending struts, localized buckling, or simultaneous disintegration. This behavior is contingent upon the manufacturing method and production quality. Surface-based lattice structures, such as TPMS, exhibit buckling-dominated failure modes that strongly depend on topology and unit-cell configuration [24]. The experimental results (Figures 10–11) indicate that the two architectures exhibit distinct deformation responses. The Pyramorph lattice predominantly failed at junctions where three or more pyramidal struts converged. At these intersections, pronounced geometric notches functioned as stress concentrators, leading to premature crack formation and resulting in unstable structural failure, as depicted in Figure 12. Once initiated, failure rapidly propagated due to the deformation of inclined struts and the delamination of layers, particularly in specimens oriented at 30° and 45°. It is well established that PLA lattices fabricated using FDM printers exhibit delamination issues. When composite (e.g. CF/PLA) TPMS lattices are used, failure often initiates via progressive crushing and interface delamination [25].

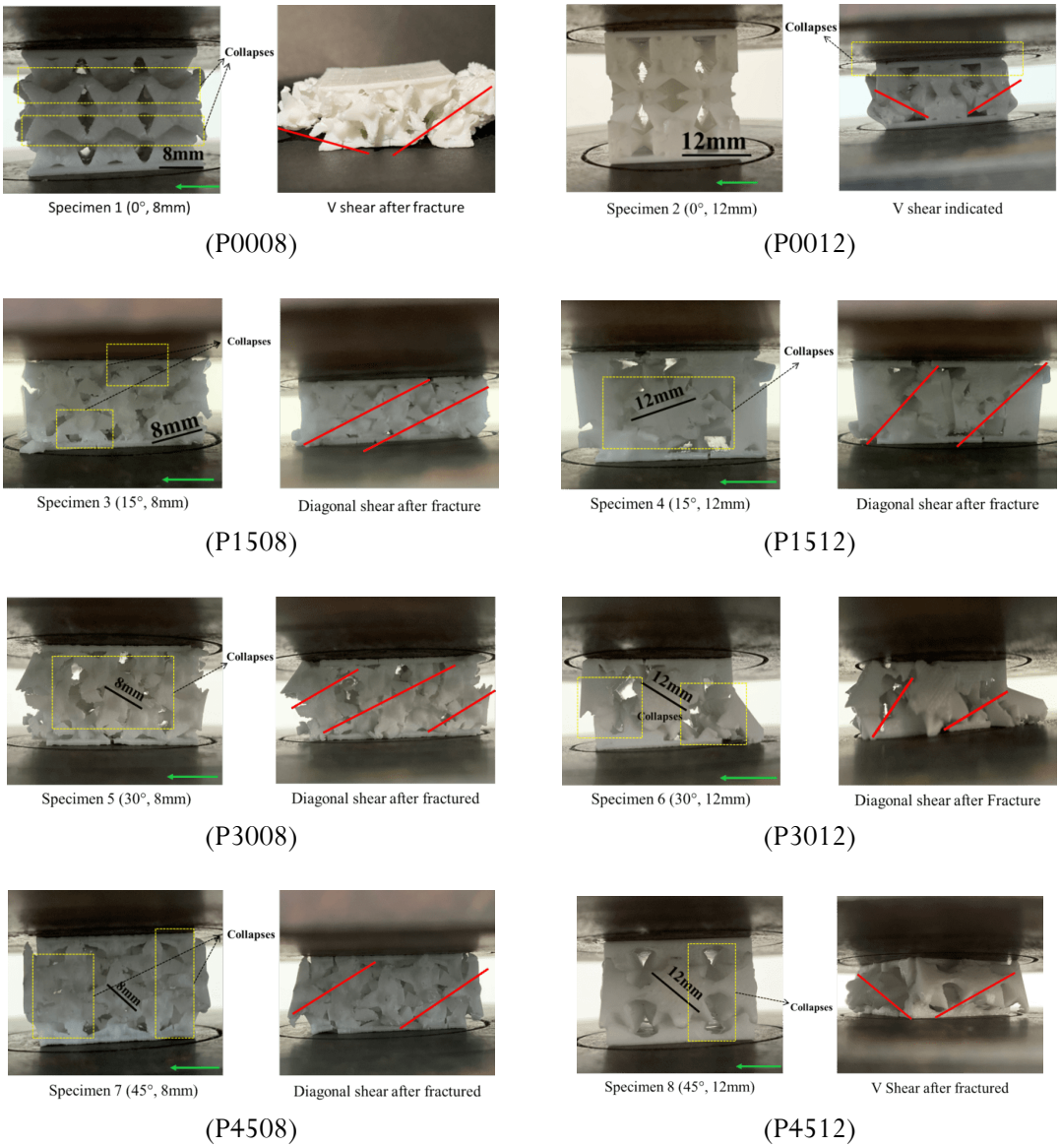

Figure 10. Experimental compressive deformation of Pyramorph Orientation 0°- 45°. The green arrow indicates the build direction

Conversely, the Topomorph Lattice exhibited a more stable and progressive compressive response. As the vertical struts reached 0°, they flexed inward and outward; however, disintegration occurred incrementally rather than simultaneously. The enhanced junction design and expanded contact surfaces at cell junctions increase stability by distributing stresses more uniformly and reducing the likelihood of localized fracture. The through-hole features further alleviate strain, rendering the material less susceptible to cuts while maintaining its structural integrity [24]. The difference highlights the importance of node design and connections to ascertain potential failure points. The Pyramorph's acute pyramidal joints introduced significant stress concentrations within the lattice, causing them to fracture in a brittle manner. Their relative densities are comparable (0.40–0.44). Designs that include vertical reinforcements or graded-node smoothing show reduced stress concentration and improve failure progression [26]. Orientation-dependent effects consistent with these observations have also been reported, where octahedron-based lattices with vertically aligned struts relative to the loading direction demonstrated superior energy absorption and load-bearing capacity compared with horizontal or uniform configurations [2], [27].

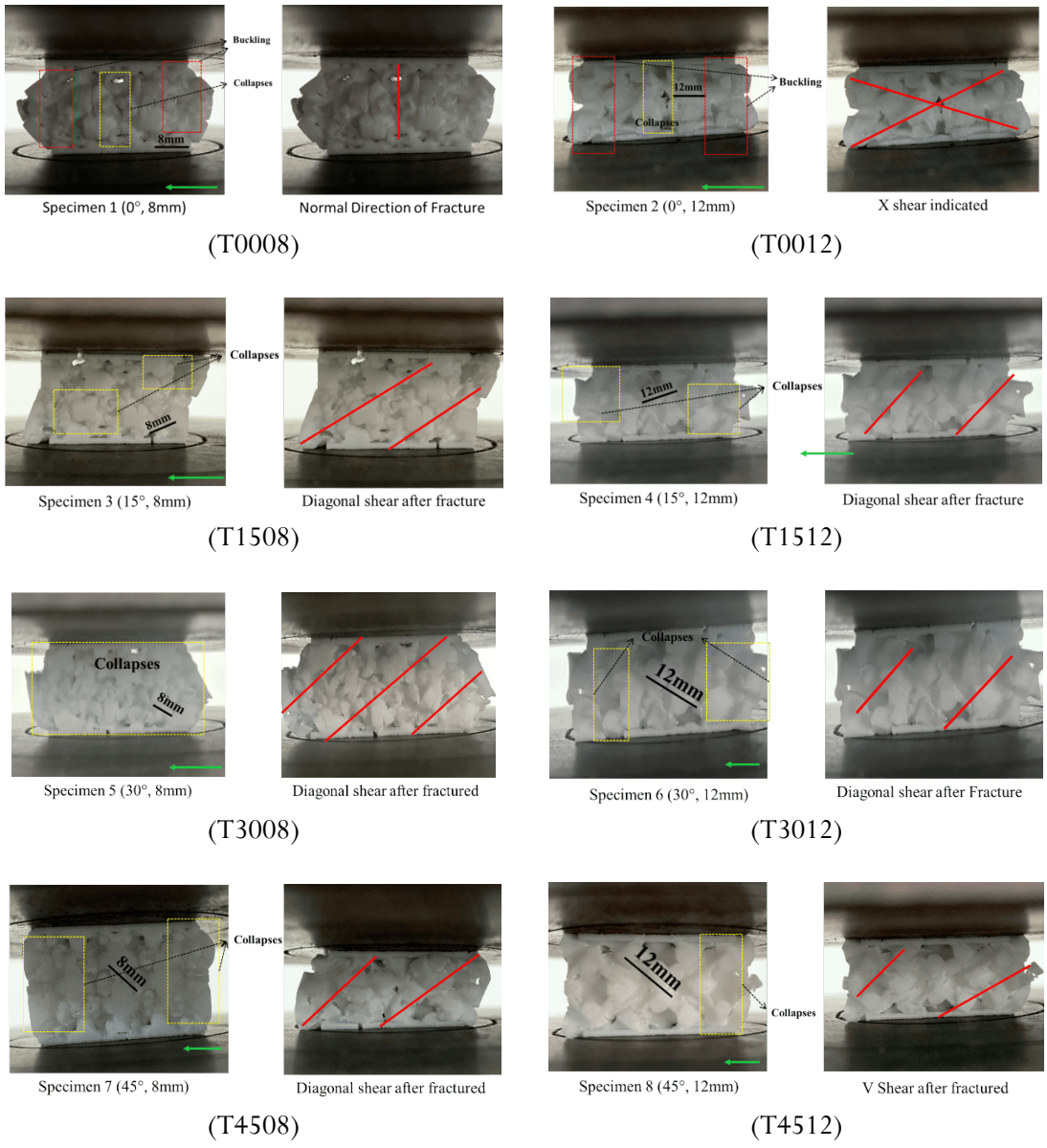

Figure 11. Experimental compressive deformation of Topomorph Orientation 0°- 45°. The green arrow indicates the build direction

Pyramorph primarily fails due to notch-induced collapse and interlayer delamination. In Topomorph, the primary modes of failure are progressive crushing and localized buckling. These results demonstrate the significance of junction morphology and connectivity as essential components of lattice design for structural applications.

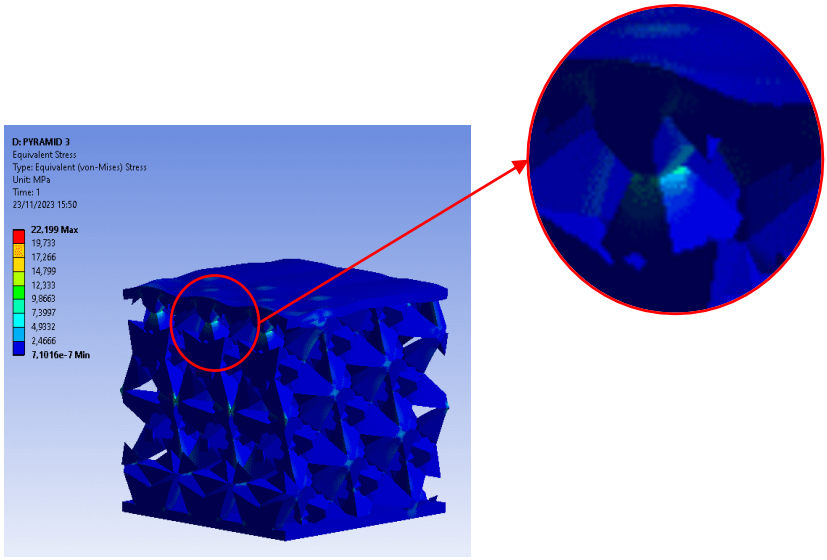

Figure 12. Stress concentration occurs on cell joint of Pyramorph Lattice

The local stress concentration found at the Pyramorph-type joints (Figure 12) is consistent with recent research on lattice structures with geometrically notched features. It has been reported that notch geometry in truss-based lattices significantly increases local stress levels and alters failure modes, often resulting in premature joint failure [28]. Furthermore, quantitative studies have shown that surface imperfections and notch shapes can increase the local stress concentration factor (SCF), which significantly affects the strength and fatigue behaviour of parts manufactured using AM methods. It has also been shown that graded smoothing and local reinforcement strategies are effective in mitigating notch sensitivity and reducing the likelihood of stress-induced failure [29]. This is similar to what is applied to Topomorph-type lattices, where the junction design reduces the tendency for sudden failure. This result also aligns with previous research related to FEA–Experiment comparisons on lattices, which revealed that numerical models typically show stress concentration at the junction sections shaped like notches, whereas experimental specimens often fail earlier in these areas due to manufacturing flaws [30], [31]. Therefore, the high local stress predicted by numerical analysis at the Pyramorph nodes is consistent with FEA reference sources and experiments that investigate notch-driven failure.

3.2 Load deformation result

The uniaxial compression tests showed that the Pyramorph and Topomorph Lattices acted differently. Each had three stages: a linear elastic region (steep initial rise), a plateau region where the structure slowly breaks down, and densification, where stress sharply rises due to cell compaction (Figures 13-14) [32], [33]. The 45° orientation of the Pyramorph lattice had the maximum yield strength, which were approximately 7–8 MPa, or about 60% higher than the other orientations. The weakest point was at 30°, indicating that load transmission paths are less effective when the struts are not lined up with the loading direction [34]. There was also a consistent size effect: 8 mm cells were stronger than 12 mm cells in all orientations. This shows how finer cell design can help keep cells from buckling [35]. But the plateau length was not consistent, perhaps because of localized instabilities at cell junctions and inter-layer delamination that are common in FDM-printed PLA structures [32].

On the other hand, the Topomorph Lattice always consistently outperformed the Pyramorph in terms of strength and energy absorption. The yield strengths were between 15 to 20 MPa, which is more than twice as high as those of Pyramorph samples. The Topomorph had wide, stable plateau areas up to $\varepsilon = 0.3–0.35$. This indicates that it had superior control over how it changed shape and how stress was spread out over time before densification [36]. This performance is attributed to its better load-bearing structure and through-hole characteristics that retain connections while lowering stress concentration [33], [37]. Similar enhancement in energy absorption demonstrated that integrating cylindrical TPMS with auxetic PSHM structures increased energy absorption density by up to 77.6% compared to single TPMS models [27]. The Pyramorph lattice typically failed because the inclined struts bowed and the printed layers came apart, especially when the layers were at a steeper inclination (30°–45°). The Topomorph Lattice, on the other hand, demonstrated progressive crushing and strut fracture with little layer separation, which demonstrated a higher load-bearing capacity and was stronger [32], [36].

The large deviation observed among specimens at high strain levels in Figures 13–14 is consistent with the compression behaviour commonly reported for additively manufactured lattice structures. At low and moderate strain, the response of the lattice is generally governed by elastic deformation and early-stage buckling, producing similar trends among specimens with identical relative density. In contrast, the mechanical properties become very sensitive to printing errors as the deformation enters the plateau and densification stages. Studies have shown that FDM-printed lattices experience progressive interlayer debonding, filament waviness, micro-void activation, and layer delamination at elevated strains, all of which reduce stiffness more rapidly than predicted by numerical models [38], [39]. Such defects are not captured in idealized CAD-based FEA models, which explains why the simulated curves remain higher while the experimental curves begin to diverge more significantly at strains above approximately 0.2–0.3 [21], [40]. In addition, orientation effects intensify the discrepancy: when the loading direction shifts away from 0°, bending, torsional deformation, and secondary buckling occur earlier, amplifying the variation between specimens. Similar orientation-dependent instability and divergence at high strain have been reported in several studies evaluating the unit-cell structure and compressive behaviour of additive manufacturing lattices [38], [41]. Therefore, the differences seen in Figures 13–14 are theoretically consistent with the collapse sequence of cellular materials and the known high-strain sensitivity of FDM-printed PLA lattice structures.

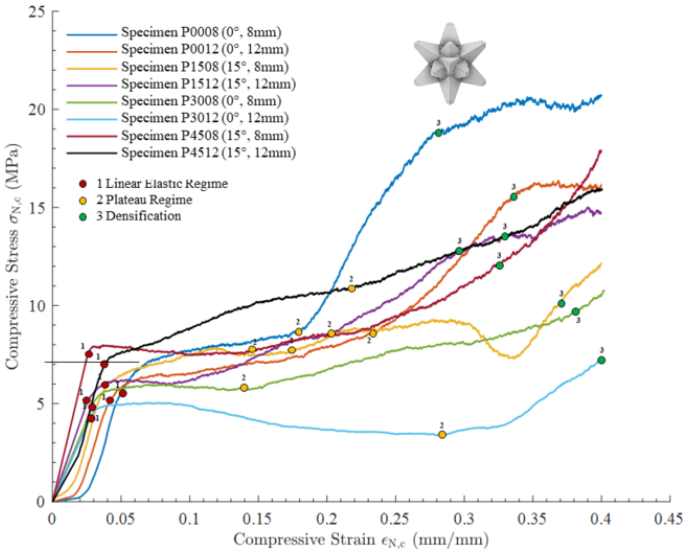

Figure 13. Experimental stress-strain curves of the compression tests on the Pyramorph lattice structures FDM Based

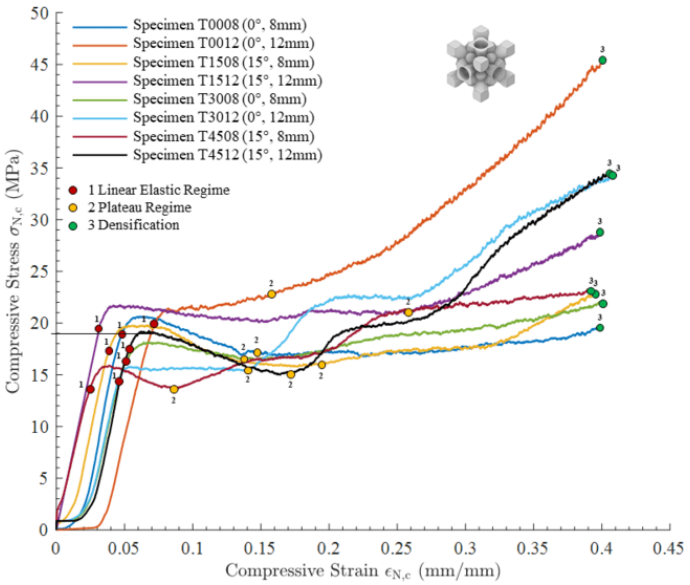

Figure 14. Experimental stress-strain curves of the compression tests on the Topomorph Lattice structures FDM Based

Overall, these results reveal that the type of lattice, the size of the cells, and the direction of the cells all work together to affect how well the material can take being compressed. The Topomorph Lattice with 8 mm cells and a 0° orientation exhibited the highest strength (around 20 MPa) and energy absorption. This makes it a promising candidate for structural applications that need to be crashworthy or biological scaffolds that can carry weight and need to be stiff and let energy out [33], [35], [36].

3.3 Correlation between experimental and numerical predictions

Figures 15 and 16 illustrate the compressive strengths that were found by experiments and finite element analysis (FEA) for both Pyramorph and Topomorph Lattices with cell sizes of 8 mm and 12 mm, respectively. The general patterns between simulation and experiment are similar, as the Topomorph Lattices always show better compressive strength than the Pyramorph lattices for all cell sizes. Recent studies have also shown that topology-optimized designs work better than regular lattices [42]. For the 8 mm cell size (Figure 15), the Topomorph at 0° (T0008) attained the maximum compressive strength, measuring approximately 20.5 MPa experimentally and nearly 37 MPa in finite element analysis (FEA), signifying an approximate 80% overestimation by the simulation. Conversely, the Pyramorph at 30°/12 mm (P3012) had the lowest compressive strength, measuring approximately 4.2 MPa empirically compared to around 9.2 MPa in finite element analysis, which is more than double the observed value. Such disparities are thoroughly established when idealized FEA models overlook process-induced imperfections [43].

For the 12 mm cell size (Figure 16), the general ranking remains consistent, with Topomorph 0° outperforming others (21 MPa experimentally vs. 28 MPa in FEA), while Pyramorph 30° remains the weakest (4.9–7.3 MPa experimental vs. 7.7 MPa FEA). Interestingly, the difference between simulation and experiment was narrower for 12 mm cells than for 8 mm cells, suggesting that manufacturing defects (e.g., staircasing and filament resolution limits) disproportionately affect smaller cells. This trend is supported by recent lattice studies, where finer cells are more sensitive to geometric inaccuracies during additive manufacturing [44].

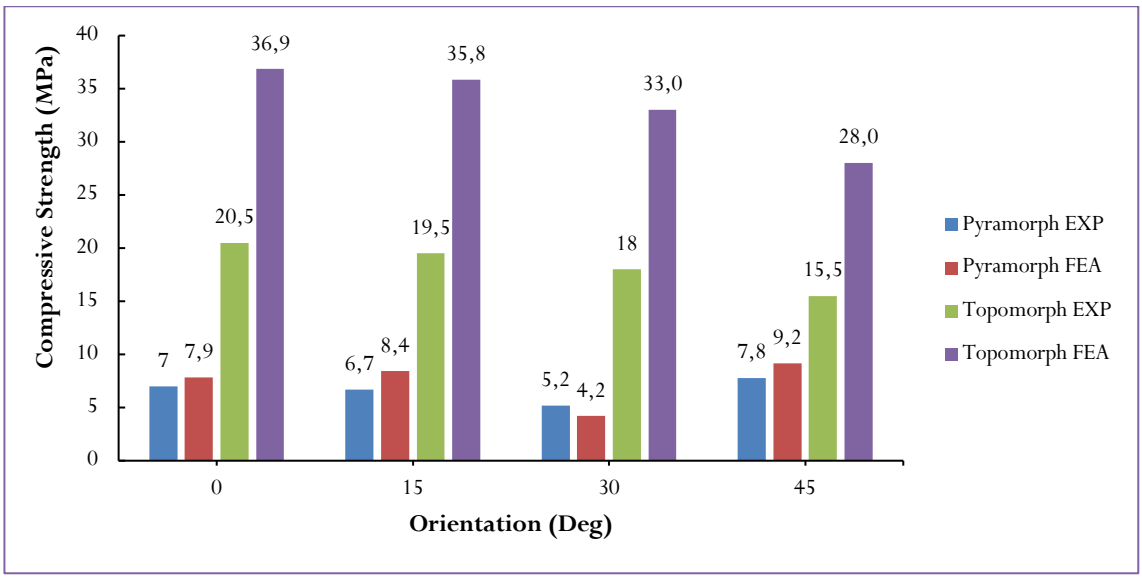

Figure 15. Maximum numerical vs experimental compressive strength of Pyramorph and Topomorph Orientation 0°- 45° Cell Size 8 mm

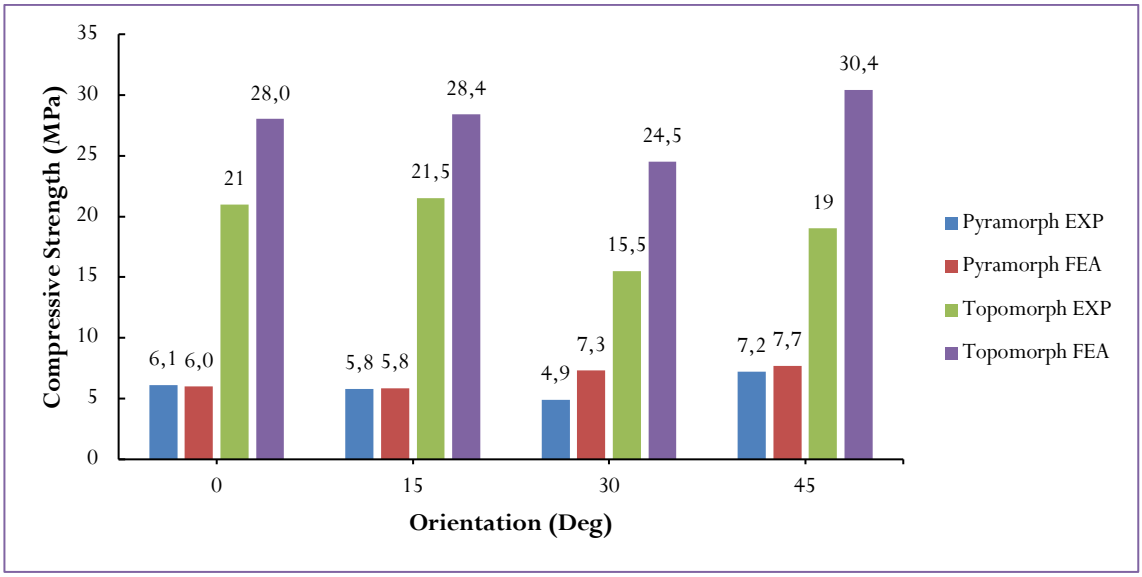

Figure 16. Maximum numerical vs experimental compressive strength of Pyramorph and Topomorph Orientation 0°- 45° Cell Size 12 mm

In this study, defect modelling, such as porosity and interlayer adhesion, was not included in the finite element simulation. The main focus of the numerical analysis was to compare the idealized load-bearing behaviour of the two lattice geometries under identical boundary conditions, rather than to replicate the full manufacturing imperfections of FDM-printed parts. Incorporating defect modelling would require additional characterization steps such as micro-CT scanning, porosity mapping, or probabilistic parameter inputs, which were beyond the scope of this comparative study. Even so, the differences observed between the numerical and experimental results align with the expected influence of these defects, as discussed in the literature. Future studies could use defect-based modeling to provide a more detailed view of the printed lattice structures.

The consistent overestimation evident in the FEA results is mostly due to discrepancies between the idealized simulation models and the real fabricated specimens. Within the numerical scheme, PLA was characterized as a fully bonded, linear elastic material; however, the FDM-printed samples

inherently possessed micro-defects, voids, and compromised interlayer adhesion, which diminished their load-bearing capacity. The CAD/FEA models inherently smooth sharp corners and disregard staircase effects produced during printing; these characteristics, however, serve as local stress concentrators and crack initiators in actual specimens, resulting in early failure [44]. Notwithstanding these quantitative disparities, the simulations effectively replicated the overarching experimental findings across both cellular topologies and orientations. The Topomorph Lattices consistently surpassed the Pyramorph counterparts due to their enhanced junction connectivity and greater stress redistribution. Furthermore, specimens with smaller cells (8 mm) often demonstrated greater strengths than those with larger cells; nevertheless, they also displayed larger discrepancies between experimental and numerical results because of the increased impact of manufacturing errors at finer scales. The orientation significantly affected the response: 0° consistently produced the most robust Topomorph specimens, but the Pyramorph occasionally attained its peak strength at 45°, a phenomenon associated with the alignment of load paths in inclined struts. These anisotropy-driven behaviors are consistent with broader findings in bio-inspired lattice research, where hybrid triply periodic minimal surface (TPMS) structures designed to mimic trabecular bone anisotropy have been shown to achieve an improved balance between stiffness and adaptability, thereby reinforcing the importance of controlled orientation and topology in attaining reliable structural performance [27].

The difference between the numerical and experimental results in the Topomorph Lattice can be traced back to the inherent characteristics of topology-optimized and curved geometries. It has been reported that finite element analysis (FEA) models of additively manufactured components typically predict higher mechanical responses, as idealized CAD geometries do not capture interlayer gaps, porosity, and surface quality deficiencies commonly associated with fused deposition modeling (FDM) processes [45]. When a lattice has more complex features, such as curved surfaces combined with through-holes, small defects become influential and can redirect the stress flow within the structure. Comparable effects have been documented in triply periodic minimal surface (TPMS) lattices, where even small geometric deviations were sufficient to initiate early strain localization and reduce compressive strength relative to numerical predictions [12]. Similarly, experimental results for AM lattices always fall below FEA due to defect amplification and stress accumulation at the node regions[46]. These explanations support the finding in the Topomorph Lattice, where the difference between the numerical and experimental results was greater than in the Pyramorph.

The differences observed between the two lattices can be explained by the way their geometries carry and distribute the load. The Topomorph has smoother junctions and higher node connectivity, which gives it more continuous load paths and allows the stresses to spread more evenly through the structure. This reduces the chance of a single point becoming overloaded. The through-holes also help redistribute the local stresses around the joints, so the material does not fail abruptly when the strain increases. On the other hand, the Pyramorph has sharp node angles and inclined struts, which create strong stress concentrations at the corners. These areas act as natural crack starters and lead to early buckling and delamination, especially under off-axis loading. This is the reason why the Pyramorph tends to fail more suddenly, while the Topomorph shows a more gradual collapse. The effect of orientation also follows this mechanism: at 0°, the load is aligned with the main struts, but at higher angles more bending and shear appear, making the differences between both geometries easier to see.

3.4 Study limitation

While the study's findings generally exhibit consistent patterns across all orientations and cell dimensions, a limitation inherent in the experimental design warrants consideration. Each test condition was represented by a single printed specimen. This constraint primarily stemmed from considerations of fabrication duration, material consumption, and the project's scope, which

prioritized the comparative analysis of the geometric characteristics of the two lattice configurations over the establishment of statistical variance. Consequently, standard deviation and error bars were not included in the graphical representations of the results. Nevertheless, the experimental results exhibited a discernible pattern, which corresponded closely with the numerical forecasts and the established deformation characteristics of FDM-derived lattice structures. The concordance observed among the finite element analysis (FEA) trends, the failure observations, and the comparative assessment of the two geometries strengthens the credibility of the conclusions. Subsequent investigations might incorporate multiple replicates for each configuration to facilitate a more comprehensive assessment of sample-to-sample variability.

4. Conclusion

This study evaluated two distinct lattice geometries, including the Pyramorph, which was inspired from pyramidal forms, and the Topomorph, which was generated using a topology-optimization approach and reconstructed using the CAD-based unit-cell patterning. Both lattice types were manufactured with matched relative densities (0.40–0.44) to ensure a fair and consistent comparison across different cell sizes and orientations. The Topomorph consistently demonstrated superior compressive performance under all test conditions, based on the experimental results. Its yield strength ranged from 15 to 20 MPa, and also exhibited a wider and more stable plateau strain of approximately $\varepsilon \approx 0.35$, while the Pyramorph remained in the range of 7–8 MPa. The highest strength, which reached approximately 20.5 MPa, was obtained by the Topomorph specimen with a cell size of 8 mm at 0°, indicating strong potential for load-bearing and energy-absorbing applications.

Notable differences in structural behaviour were observed during the failure investigation. The Pyramorph exhibited heightened susceptibility to initial damage due to its acute node angles and sloped struts, which generated significant stress concentrations that precipitated buckling and delamination, particularly at higher build orientations. These features served as natural fracture initiation sites, resulting in a more abrupt structural failure. In contrast, the Topomorph exhibited a different failure behavior. The improved interconnections, augmented connectivity, and presence of through-holes contributed to a more even load distribution across the cellular structure. Deformation progressed through gradual crushing and localized buckling, as opposed to an abrupt failure. This comparative analysis highlights the influence of node configuration, joint continuity, and the overall load-path distribution on the stability and reliability of a lattice system.

This study focused exclusively on compressive loading as it represents the most common failure mode for lattice structures and provides a clear comparison between the two geometries. Other loading modes, such as tensile, bending, or fatigue, were not investigated in this work. Such tests would require different specimen designs, different boundary conditions, and additional manufacturing time. Nevertheless, the method introduced in this paper can be applied to other loading cases, and future work may extend the evaluation to multiple loading modes or different materials and manufacturing processes. This would provide a broader understanding of how Pyramorph and Topomorph behave under more complex mechanical conditions.

Author's declaration

Author contribution

Ahmad Anas Arifin: Conceptualization, Data curation, Investigation, Methodology and Writing – original draft. **I Made Londen Batan**: Supervision and Validation. **Michele Bici**: Formal analysis, Writing – review & editing. **Arif Wahjudi**: Formal analysis, Supervision and Visualization. **Agus Sigit Pramono**: Conceptualization, Software and Supervision.

Funding statement

This research was supported by the Indonesian Education Scholarship (BPI), the Center for Higher Education Funding and Assessment (PPAPT), the Ministry of Higher Education, Science, and Technology of the Republic of Indonesia (Kemdiktisaintek), and the Indonesian Endowment Fund for Education (LPDP), Ministry of Finance of the Republic of Indonesia.

Data availability

All related data that are not presented in the article are available and can be shared upon request by e-mail to the corresponding author.

Acknowledgements

The first author thankfully acknowledges the financial support provided by Indonesian Education Scholarship (BPI), Center for Higher Education Funding and Assessment (PPAPT), Ministry of Higher Education, Science, and Technology of the Republic of Indonesia (Kemdiktisaintek), and Indonesian Endowment Fund for Education (LPDP), Ministry of Finance of the Republic of Indonesia.

Competing interest

The authors declare that they are NOT affiliated with or involved in any organization or entity that has a financial interest (such as honoraria; educational grants; participation in speakers' bureaus; membership, employment, consulting, stock ownership, or other equity interests; and expert testimony or patent licensing arrangements), or non-financial interest (such as personal or professional relationships, affiliations, knowledge, or beliefs) in the subject matter or materials discussed in this manuscript.

Ethical clearance

This research does not involve humans as subjects.

AI statement

The language use in this article has been validated and verified by an English language expert, and none of the AI-generated sentences are included.

Publisher's and Journal's note

Universitas Negeri Padang as the publisher, and Editor of Teknomekanik state that there is no conflict of interest towards this article publication.

References

[1] M. Bici *et al.*, "Development of a multifunctional panel for aerospace use through SLM additive manufacturing," *Procedia CIRP*, vol. 67, pp. 215–220, 2018, https://doi.org/10.1016/j.procir.2017.12.202

[2] H. Monjezi, M. Asghari, and K. Mohammadi, "Hybrid layered octahedron-based lattice structures, deformation pattern and mechanical properties," *Results in Engineering*, vol. 26, p. 105082, 2025, https://doi.org/10.1016/j.rineng.2025.105082

[3] A. Ahmad, L. Belluomo, M. Bici, and F. Campana, "Bird's Eye View on Lattice Structures: Design Issues and Applications for Best Practices in Mechanical Design," *Metals (Basel)*, vol. 13, no. 10, 2023, https://doi.org/10.3390/met13101666

[4] C. Pan, Y. Han, and J. Lu, "Design and optimization of lattice structures: A review," *Applied Sciences*, vol. 10, no. 18, p. 6374, 2020. https://doi.org/10.3390/app10186374

[5] M. Zhao, D. Z. Zhang, Z. Li, T. Zhang, H. Zhou, and Z. Ren, "Design, mechanical properties, and optimization of BCC lattice structures with taper struts," *Composite Structures*, vol. 295, p. 115830, 2022. https://doi.org/10.1016/j.compstruct.2022.115830

[6] Y. Lin *et al.*, "Influence of Density Gradient on the Compression of Functionally Graded BCC Lattice Structure," *Materials*, vol. 16, no. 2, 2023, https://doi.org/10.3390/ma16020520

[7] T. Tancogne-Dejean and D. Mohr, "Elastically-isotropic truss lattice materials of reduced plastic anisotropy," *International Journal of Solids and Structures*, vol. 138, pp. 24–39, 2018, https://doi.org/10.1016/j.ijsolstr.2017.12.025

[8] J. Feng, B. Liu, Z. Lin, and J. Fu, "Isotropic octet-truss lattice structure design and anisotropy control strategies for implant application," *Materials and Design*, vol. 203, p. 109595, 2021, https://doi.org/10.1016/j.matdes.2021.109595

[9] S. Xu, J. Shen, S. Zhou, X. Huang, and Y. M. Xie, "Design of lattice structures with controlled anisotropy," *Materials and Design*, vol. 93, pp. 443–447, 2016, https://doi.org/10.1016/j.matdes.2016.01.007

[10] A. Kumar, L. Collini, A. Daurel, and J. Y. Jeng, "Design and additive manufacturing of closed cells from supportless lattice structure," *Additive Manufacturing*, vol. 33, no. January, p. 101168, 2020, https://doi.org/10.1016/j.addma.2020.101168

[11] S. E. Alkhatib, A. Karrech, and T. B. Sercombe, "Isotropic energy absorption of topology optimized lattice structure," *Thin-Walled Structures*, vol. 182, no. June 2022, p. 110220, 2023, https://doi.org/10.1016/j.tws.2022.110220

[12] Y. Li, D. Jiang, R. Zhao, X. Wang, L. Wang, and L. C. Zhang, "High Mechanical Performance of Lattice Structures Fabricated by Additive Manufacturing," *Metals*, vol. 14, no. 10, 2024, https://doi.org/10.3390/met14101165

[13] M. Peto, E. Ramírez-Cedillo, A. Hernández, and H. R. Siller, "Structural design optimization of knee replacement implants for Additive Manufacturing," *Procedia Manufacturing*, vol. 34, no. July, pp. 574–583, 2019, https://doi.org/10.1016/j.promfg.2019.06.222

[14] N. Letov and Y. F. Zhao, "A geometric modelling framework to support the design of heterogeneous lattice structures with non-linearly varying geometry," *Journal of Computational Design and Engineering*, vol. 9, no. 5, pp. 1565–1584, 2022, https://doi.org/10.1093/jcde/qwac076

[15] J. G. Lee, Y. B. Jun, and K. Hur, "Octahedron subgroups and subrings," *Mathematics*, vol. 8, no. 9, pp. 1–33, 2020, https://doi.org/10.3390/MATH8091444

[16] A. A. Arifin, I. M. L. Batan, M. Bici, A. Wahjudi, and A. S. Pramono, "Investigation of discrepancies in isotropic material and structural properties in lattice frameworks," *Mechanical Engineering for Society and Industry*, vol. 5, no. 1, pp. 245–256, 2025, https://doi.org/10.31603/mesi.13018

[17] A. A. Arifin, I. M. L. Batan, M. Bici, A. Wahjudi, and A. S. Pramono, "Isotropic Body-Centered Cubic (BCC) Lattice Structure Design," in *Smart Innovation in Mechanical Engineering*, A. El Kharbachi, I. D. Wijayanti, P. Suwarta, and I. Tolj, Eds., Singapore: Springer Nature Singapore, 2025, pp. 45–53. https://doi.org/10.1007/978-981-97-7898-0_6

[18] I. Gibson, D. Rosen, B. Stucker, and M. Khorasani, *Additive Manufacturing Technologies*. Cham: Springer International Publishing, 2021. https://doi.org/10.1007/978-3-030-56127-7

[19] N. Letov and Y. F. Zhao, "A geometric modelling framework to support the design of heterogeneous lattice structures with non-linearly varying geometry," *Journal of Computational Design and Engineering*, vol. 9, no. 5, pp. 1565–1584, Oct. 2022, https://doi.org/10.1093/jcde/qwac076

[20] L. Piegl and W. Tiller, "Conics and Circles," pp. 281–331, 1997, https://doi.org/10.1007/978-3-642-59223-2_7

[21] M. Saleh, S. Anwar, A. M. Al-Ahmari, and A. Alfaify, "Compression performance and failure analysis of 3D-printed carbon fiber/PLA composite TPMS lattice structures," *Polymers*, vol. 14, no. 21, p. 4595, 2022. https://doi.org/10.3390/polym14214595

[22] M. M. Rahman, J. Sultana, S. Bin Rayhan, and A. Ahmed, "Optimization of FDM manufacturing parameters for the compressive behavior of cubic lattice cores: an experimental approach by Taguchi method," *The International Journal of Advanced Manufacturing Technology*, vol. 129, no. 3, pp. 1329–1343, 2023. https://doi.org/10.1007/s00170-023-12342-9

[23] A. Kumar, L. Collini, A. Daurel, and J. Y. Jeng, "Design and additive manufacturing of closed cells from supportless lattice structure," *Additive Manufacturing*, vol. 33, no. January, p. 101168, 2020, https://doi.org/10.1016/j.addma.2020.101168

[24] G. J. Shah, A. Nazir, S.-C. Lin, and J.-Y. Jeng, "Design for Additive Manufacturing and Investigation of Surface-Based Lattice Structures for Buckling Properties Using Experimental and Finite Element Methods.," *Materials (Basel, Switzerland)*, vol. 15, no. 11, Jun. 2022, https://doi.org/10.3390/ma15114037

[25] M. Saleh, S. Anwar, A. M. Al-Ahmari, and A. Alfaify, "Compression Performance and Failure Analysis of 3D-Printed Carbon Fiber/PLA Composite TPMS Lattice Structures," *Polymers*, vol. 14, no. 21, 2022, https://doi.org/10.3390/polym14214595

[26] S. O. Obadimu and K. I. Kourousis, "Compressive behaviour of additively manufactured lattice structures: A review," *Aerospace*, vol. 8, no. 8, 2021, https://doi.org/10.3390/aerospace8080207

[27] A. Malekshahi, S. J. Salami, H. Geramizadeh, and S. Dariushi, "A novel combined tubular 3D-printed lattice structures with coupling effects for enhancing energy absorption," *Results in Engineering*, vol. 26, p. 105350, 2025, https://doi.org/10.1016/j.rineng.2025.105350

[28] G. Meyer, H. Wang, and C. Mittelstedt, "Influence of geometrical notches and form optimization on the mechanical properties of additively manufactured lattice structures," *Materials & Design*, vol. 222, p. 111082, 2022. https://doi.org/10.1016/j.matdes.2022.111082

[29] V. Chmelko, M. Harakaľ, P. Žlábek, M. Margetin, and R. Ďurka, "Simulation of Stress Concentrations in Notches," *Metals*, vol. 12, no. 1. 2022. https://doi.org/10.3390/met12010043

[30] N. Kladovasilakis, K. Tsongas, and D. Tzetzis, "Mechanical and FEA-assisted characterization of fused filament fabricated triply periodic minimal surface structures," *Journal of Composites Science*, vol. 5, no. 2, p. 58, 2021. https://doi.org/10.3390/jcs5020058

[31] M. Zheng, K. Ghabraie, Y. Yang, J. Elambasseril, W. Xu, and Y. Wang, "Quantitative surface characterisation and stress concentration of additively manufactured NiTi lattice struts," *The International Journal of Advanced Manufacturing Technology*, vol. 130, no. 9, pp. 4861–4882, 2024, https://doi.org/10.1007/s00170-024-13024-w

[32] Y. Xu, T. Li, X. Cao, Y. Tan, and P. Luo, "Compressive Properties of 316L Stainless Steel Topology-Optimized Lattice Structures Fabricated by Selective Laser Melting," *Advanced Engineering Materials*, vol. 23, no. 3, p. 2000957, Mar. 2021, https://doi.org/10.1002/adem.202000957

[33] L. Zhang *et al.*, "Topology-optimized lattice structures with simultaneously high stiffness and light weight fabricated by selective laser melting: Design, manufacturing and

characterization," *Journal of Manufacturing Processes*, vol. 56, pp. 1166–1177, 2020, https://doi.org/10.1016/j.jmapro.2020.06.005

[34] B. Jagadeesh and M. Duraiselvam, "Investigations on the compressive behaviour of novel cell size graded primitive lattice structure produced by Metal Additive Manufacturing," *Materials Letters*, vol. 333, p. 133643, 2023, https://doi.org/10.1016/j.matlet.2022.133643

[35] J. Hu, A. T. L. Tan, H. Chen, and X. Hu, "Superior compressive properties of 3D printed plate lattice mechanical metamaterials," *International Journal of Mechanical Sciences*, vol. 231, p. 107586, 2022, https://doi.org/10.1016/j.ijmecsci.2022.107586

[36] W. Song *et al.*, "Mechanical Behavior of Topology-Optimized Lattice Structures Fabricated by Additive Manufacturing," *Materials*, vol. 18, no. 15, p. 3614, 2025, https://doi.org/10.3390/ma18153614

[37] P. Dong, J. Hu, C. Lin, W. Ding, J. Liu, and Y. Liu, "Topology-optimized lattice enhanced cementitious composites," *Materials & Design*, vol. 244, p. 113155, 2024, https://doi.org/10.1016/j.matdes.2024.113155

[38] S. O. Obadimu and K. I. Kourousis, "Compressive Behaviour of Additively Manufactured Lattice Structures: A Review," *Aerospace*, vol. 8, no. 8. 2021. https://doi.org/10.3390/aerospace8080207

[39] W. Xu *et al.*, "Design and performance evaluation of additively manufactured composite lattice structures of commercially pure Ti (CP-Ti).," *Bioactive materials*, vol. 6, no. 5, pp. 1215–1222, May 2021, https://doi.org/10.1016/j.bioactmat.2020.10.005

[40] W. Radlof, C. Benz, and M. Sander, "Numerical and experimental investigations of additively manufactured lattice structures under quasi-static compression loading," *Material Design & Processing Communications*, vol. 3, no. 3, p. e164, Jun. 2021, https://doi.org/https://doi.org/10.1002/mdp2.164

[41] D. Liović *et al.*, "A Study on the Compressive Behavior of Additively Manufactured AlSi10Mg Lattice Structures," *Materials*, vol. 17, no. 21. 2024. https://doi.org/10.3390/ma17215188

[42] Y. Deng, B. Li, Z. Huang, Y. Lin, and Y. Li, "Experimental and numerical studies on the compression responses of novel mixed lattice structures," *Materials Today Communications*, vol. 33, p. 104439, 2022. https://doi.org/10.1016/j.mtcomm.2022.104439

[43] X. Cao *et al.*, "Compression experiment and numerical evaluation on mechanical responses of the lattice structures with stochastic geometric defects originated from additive-manufacturing," *Composites Part B: Engineering*, vol. 194, p. 108030, 2020. https://doi.org/10.1016/j.compositesb.2020.108030

[44] M. Amirpour and M. Battley, "Study of manufacturing defects on compressive deformation of 3D-printed polymeric lattices," *The International Journal of Advanced Manufacturing Technology*, vol. 122, no. 5, pp. 2561–2576, 2022. https://doi.org/10.1007/s00170-022-10062-0

[45] I. Echeta, B. Dutton, R. K. Leach, and S. Piano, "Finite element modelling of defects in additively manufactured strut-based lattice structures," *Additive Manufacturing*, vol. 47, p. 102301, 2021, https://doi.org/10.1016/j.addma.2021.102301

[46] A. Amirian, M. Battley, O. Diegel, and M. Amirpour, "Additive manufacturing defects in polymeric lattice structures: a comprehensive analysis of morphology, distribution, and printing orientation influence," *The International Journal of Advanced Manufacturing Technology*, vol. 140, no. 9, pp. 5361–5384, 2025, https://doi.org/10.1007/s00170-025-16521-8

Nomenclature

Φ	relative density
V_L	Volume of lattice (mm^3)
V_s	Volume of solid cube (mm^3)

C	Center shift
σ	Stress (MPa)
ε	Strain
$\sigma_{N,c}$	Nominal Compressive Stress (MPa)
$\varepsilon_{N,c}$	Nominal Compressive Strain (%)
P_c	Compressive Load (N)
$A_{0,eq}$	Equivalent Cross Section Area of Cell (mm2)
u_c	Compressive displacement (mm)
h_0	Initial height (mm)
W_c	Energy absorption per unit volume calculated up to $\varepsilon = 0.4$.
$Fmax$	Maximum bearable load of the specimen (N)
F_{max}	Maximum bearable load of the specimen (N)
σ_y	Yield strength of PLA Material (63.2 MPa)
σ_{actual}	Von Mises Stress from FEA Simulation (MPa)
F_{input}	Input force (100 N)
$\sigma_{compressive\ strength}$	Compressive Strength by FEA (MPa)
A	Equivalent Cross Section Area of Cell (mm^2)